Brief Communication

MOLECULAR METABOLISM

Pleiotropic actions of IP6K1 mediate hepatic metabolic dysfunction to promote nonalcoholic fatty liver disease and steatohepatitis

Sandip Mukherjee [1], Molee Chakraborty [1], Barbara Ulmasov [2], Kyle McCommis [3], Jinsong Zhang [1], Danielle Carpenter [4], Eliwaza Naomi Msengi [1], Jake Haubner [1], Chun Guo [1], Daniel P. Pike [3], Sarbani Ghoshal [5], David A. Ford [3], Brent A. Neuschwander-Tetri [2], Anutosh Chakraborty [1,*]

ABSTRACT

Objective: Obesity and insulin resistance greatly increase the risk of nonalcoholic fatty liver disease and steatohepatitis (NAFLD/NASH). We have previously discovered that whole-body and adipocyte-specific *Ip6k1*deletion protects mice from high-fat-diet-induced obesity and insulin resistance due to improved adipocyte thermogenesis and insulin signaling. Here, we aimed to determine the impact of hepatocyte-specific and whole-body *Ip6k1* deletion *(HKO* and *Ip6k1-KO* or *KO)* on liver metabolism and NAFLD/NASH.

Methods: Body weight and composition; energy expenditure; glycemic profiles; and serum and liver metabolic, inflammatory, fibrotic and toxicity parameters were assessed in mice fed Western and high-fructose diet (HFrD) (WD: 40% kcal fat, 1.25% cholesterol, no added choline and HFrD: 60% kcal fructose). Mitochondrial oxidative capacity was evaluated in isolated hepatocytes. RNA-Seq was performed in liver samples. Livers from human NASH patients were analyzed by immunoblotting and mass spectrometry.

Results: *HKO* mice displayed increased hepatocyte mitochondrial oxidative capacity and improved insulin sensitivity but were not resistant to body weight gain. Improved hepatocyte metabolism partially protected *HKO* mice from NAFLD/NASH. In contrast, enhanced whole-body metabolism and reduced body fat accumulation significantly protected whole-body *Ip6k1-KO* mice from NAFLD/NASH. Mitochondrial oxidative pathways were upregulated, whereas gluconeogenic and fibrogenic pathways were downregulated in *Ip6k1-KO* livers. Furthermore, IP6K1 was upregulated in human NASH livers and interacted with the enzyme *O*-GlcNAcase that reduces protein *O*-GlcNAcylation. Protein *O*-GlcNAcylation was found to be reduced in *Ip6k1-KO* and *HKO* mouse livers.

Conclusion: Pleiotropic actions of IP6K1 in the liver and other metabolic tissues mediate hepatic metabolic dysfunction and NAFLD/NASH, and thus IP6K1 deletion may be a potential treatment target for this disease.

Keywords IP6K1; NAFLD/NASH; Liver; Metabolism; Hyperglycemia; *O*-GlcNAcylation

1. INTRODUCTION

A family of three mammalian inositol hexakisphosphate kinases (IP6Ks) converts the biomolecule inositol hexakisphosphate (IP6) to the inositol pyrophosphate (5-IP7) [1—5]. IP6 and 5-IP7 regulate various cellular processes including metabolism [1—4]. Of the IP6K isotypes, the functions of IP6K1 have been the most characterized *in vivo* [3,6]. IP6K1 promotes insulin secretion from pancreatic β cells [7] but impairs insulin signaling by inhibiting the insulin effector protein kinase Akt [8]. Thus, in a chronic energy-rich state, IP6K1 contributes to hyperinsulinemia and insulin resistance [8]. Moreover, IP6K1 reduces whole-body energy expenditure by inhibiting thermogenesis in adipocytes [9]. IP6K1 diminishes energy oxidation and augments fatty acid biosynthesis in adipocytes by inhibiting the metabolism-enhancing AMP-activated protein kinase (AMPK) [9,10]. IP6K1 also reduces adipose tissue- and serum levels of the insulin sensitizing and metabolically favorable adipokine adiponectin [9,10]. Consequently, whole-body (*Ip6k1-KO* or *KO*) and adipocyte-specific *Ip6k1-KO* mice display improved insulin sensitivity and energy metabolism and are protected from high-fat-diet-induced (HFD: 60% kcal from fat, no added cholesterol) obesity, hyperinsulinemia, and insulin resistance [8—10].

Obesity-induced hyperinsulinemia and insulin resistance greatly increase the risk of nonalcoholic fatty liver disease and steatohepatitis (NAFLD/NASH) [11,12]. In obesity, dysfunctional adipocytes release abnormal amounts of free fatty acids (FFAs), which are taken up by the liver, leading to lipotoxic liver injury [11,12]. This injury and the associated activated macrophages together provide a stimulus for hepatic stellate cell (HSC) activation into a fibrogenic phenotype [12—

[1]Department of Pharmacology and Physiology, Saint Louis University School of Medicine, Saint Louis, MO, 63104, USA [2]Division of Gastroenterology and Hepatology, Saint Louis University School of Medicine, Saint Louis, MO, 63104, USA [3]Department of Biochemistry, Saint Louis University School of Medicine, Saint Louis, MO, 63104, USA [4]Department of Pathology, Saint Louis University School of Medicine, Saint Louis, MO, 63104, USA [5]Department of Biological Sc. and Geology, QCC-CUNY, Bayside, NY, USA

*Corresponding author. E-mail: anutosh.chakraborty@health.slu.edu (A. Chakraborty).

Received August 24, 2021 • Revision received October 11, 2021 • Accepted October 23, 2021 • Available online 28 October 2021

https://doi.org/10.1016/j.molmet.2021.101364

Abbreviations

NAFLD	Nonalcoholic fatty liver disease
NASH	Nonalcoholic steatohepatitis
Ip6k1-KO	whole body Inositol hexakisphosphate kinase-1 knock out
HKO	Hepatocyte specific *Ip6k1 knock out*
IP6	Inositol hexakisphosphate
5-IP7	5-diphosphoinositol pentakisphosphate or 5-inositol pyrophosphate
AdKO	Adipocyte specific *Ip6k1 knockout*
WD	Western Diet
HFrD	High fructose diet
LTCDS	Liver Tissue Cell Distribution System
WT	Wild type
Lox	*Ip6k1 flox*
CLAMS	Comprehensive Lab Animal Monitoring System
NMR	Nuclear Magnetic Resonance
OCR	Oxygen consumption rate
TNP	N2-(m-Trifluoro benzyl), N6-(p-nitrobenzyl)purine
FCCP	Carbonyl cyanide-p-trifluoromethoxyphenylhydrazone
ECAR	Extracellular acidification rate
ARP	Acidic ribosomal protein large P0
GSEA	Gene set enrichment analysis
TMM	The trimmed mean of M-values
LC-MS/MS	Liquid chromatography with tandem mass spectrometry
HDMC	Phepatocellular carcinoma down-regulated mitochondrial carrier protein
DNPME	2,4-dinitrophenol-methyl ether

NAFLD Nonalcoholic fatty liver disease
NASH Nonalcoholic steatohepatitis
Ip6k1-KO whole body Inositol hexakisphosphate kinase-1 knock out
HKO Hepatocyte specific *Ip6k1 knock out*
IP6 Inositol hexakisphosphate
5-IP7 5-diphosphoinositol pentakisphosphate or 5-inositol pyrophosphate
AdKO Adipocyte specific *Ip6k1 knockout*
WD Western Diet
HFrD High fructose diet
LTCDS Liver Tissue Cell Distribution System
WT Wild type
Lox *Ip6k1 flox*
CLAMS Comprehensive Lab Animal Monitoring System
NMR Nuclear Magnetic Resonance
OCR Oxygen consumption rate
TNP N2-(m-Trifluoro benzyl), N6-(p-nitrobenzyl)purine
FCCP Carbonyl cyanide-p-trifluoromethoxyphenylhydrazone
ECAR Extracellular acidification rate
ARP Acidic ribosomal protein large P0
GSEA Gene set enrichment analysis
TMM The trimmed mean of M-values
LC-MS/MS Liquid chromatography with tandem mass spectrometry
HDMC Phepatocellular carcinoma down-regulated mitochondrial carrier protein
DNPME 2,4-dinitrophenol-methyl ether

14]. Moreover, obesity-induced hyperinsulinemia causes pathway-selective insulin resistance, leading to reduced glucose uptake but increased gluconeogenesis and *de novo* lipogenesis in the hepatocytes [15]. Altered cholesterol and fructose metabolism in hepatocytes also contribute to the development of NAFLD/NASH [11,12,16,17]. Thus, obesity-induced liver disease often begins with benign steatosis that can subsequently progress to steatohepatitis with inflammation and fibrosis and, in some individuals, cirrhosis and hepatocellular carcinoma, with cardiovascular disease being a common comorbidity [11,18]. Although there are no FDA-approved drugs to treat NASH, many current therapies in development focus on improving energy metabolism, insulin sensitivity, inflammation, and fibrosis [11,12,19,20]. A protein or pathway that has pleiotropic beneficial effects on these processes may be an ideal treatment target for NAFLD/NASH.

Despite being the major inositol pyrophosphate-generating enzyme in the hepatocytes [8,9], the role of IP6K1 in hepatic metabolism and in the etiology of NAFLD/NASH remains poorly understood. Therefore, by using a choline-deficient Western diet and a high fructose diet (HFrD) (WD: 40% kcal fat, 1.25% cholesterol and HFrD: 60% kcal fructose) to induce the full spectrum of NAFLD/NASH [21–23] and hepatic metabolic dysfunction in mice [24], we aimed to determine the impact of hepatocyte-specific and whole-body deletion of *Ip6k1* on hepatic metabolism and NAFLD/NASH. The expression of IP6K1 in human NASH liver samples was also assessed.

2. MATERIALS AND METHODS

2.1. Human liver tissue samples

Human liver studies were approved by the Saint Louis University Institutional Biosafety Committee. Frozen deidentified human liver samples from normal individuals as well as from NASH and cirrhosis patients were obtained from the Liver Tissue Cell Distribution System (LTCDS) at The University of Minnesota.

2.2. Animal diets and study designs

All animal studies were approved by the Saint Louis University Institutional Animal Care and Use Committee. *WT*, *Ip6k1-KO* [8,9], *Lox*, and *HKO* mice on C57BL6 (JAX) background were housed at 23 °C under 12-hour light/dark cycles. The mice were fed ad libitum with free access to water and were in good health condition throughout the duration of treatment. *Ip6k1-flox* (*Lox*) and albumin-*Cre* (JAX: 003574) mice were crossed to generate *HKO* mice following a standard protocol [9]. Age-matched littermates were used in all experiments.

Ten-week-old chow-fed male and female mice were fed the WD for 18 weeks. Whole body energy expenditure measurement (CLAMS) was performed at the 10th week. Insulin, pyruvate, glucagon, and glucose tolerance tests (ITT, PTT, GgTT, and GTT) were performed in WD-fed male mice at the 14th, 15th, 16th, and 17th weeks, respectively, to assess progressive insulin resistance. ITT was performed in WD-fed female mice at the 14th week. Moreover, 10-week-old chow-fed mice were fed a HFrD for 16 weeks. GgTT and ITT were performed at the 10th and 12th weeks, respectively. After the feeding period was over, the animals were fasted for 5h and euthanized. Tissues were collected for further studies.

2.3. Glucose, insulin, pyruvate, and glucagon tolerance tests

For GTT or PTT, glucose, or pyruvate (2 g/kg BW, i.p.) was injected in 16-h-fasted animals. For ITT or GgTT, insulin (0.75 U/kg BW, i.p.) or glucagon (15 μg/kg BW, i.p.) was injected in 5-h fasted mice. Blood glucose levels were measured using a glucometer by puncturing the tail veins of mice before and after the indicated time periods of injection [8,9,25].

2.4. Hematoxylin and eosin (H&E) staining and NAFLD feature scoring

Overnight-formalin-fixed tissues were processed and stained. NAFLD features were scored using a semiquantitative scoring system [26]. Steatosis was scored as: 0 (no steatosis or steatosis occupying less than 5% of the hepatic parenchyma), 1 (steatosis occupying 5–33% of the parenchyma), 2 (33–66% of parenchyma), 3 (>66% of parenchyma); hepatocyte enlargement, lobular and portal inflammatory cell infiltration were scored as: 0 (none), 1 (mild, one to two foci/200 X field), 2 (moderate, three to four foci/200 X field), and 3 (severe, more than four foci/200 X field).

2.5. Sirius red staining and analysis of the total collagen content

Paraffin-embedded liver sections were stained with 0.1% Sirius Red in saturated picric acid for 2 h. Slides were then washed in water, dehydrated with ethanol and xylene, and mounted. The degree of collagen accumulation was assessed by morphometric analysis, as described previously [27]. Briefly, about 15–20 nonoverlapping images randomly selected from each liver section were captured at 20× magnification. The same threshold was applied to all images. Sirius Red staining was quantified by digital image analysis using ImageJ software (NIH). The amount of collagen in the *Ip6k1-KO* or *HKO* livers was expressed relative to the amount of collagen in the corresponding *WT* or *Lox* control group.

2.6. Measurement of TAG, AST, ALT, LDL, and HDL

Serum was prepared immediately after blood collection and was aliquoted and frozen at −80 °C. TAG, AST, ALT, and LDL and HDL cholesterol were measured using commercial kits following the manufacturer's instructions. Hepatic lipid extraction for TAG measurement was performed following the standard protocol [28].

2.7. Mitochondrial oxygen consumption rate (OCR)

Murine primary hepatocytes were isolated as described previously [25] and plated onto 50 μg/ml of collagen (type I) coated 96-well XF plate in complete DMEM (2×10^4 cells/well). After 24 h, vehicle (DMSO: PBS, 1:3) or TNP (1 μM) was added for 2 h. Subsequently, DMEM was replaced with vehicle or TNP containing XF medium (5 mM pyruvate and 2.5 mM glucose) for 1 h. The plate was then placed in a Seahorse Analyzer. After baseline measurements, 3 sequential injections were applied to the wells: oligomycin (complex V inhibitor, 1 μg/ml), FCCP (uncoupler, 1 μM), and antimycin A (complex III inhibitor, 0.8 μM) combined with rotenone (complex I inhibitor, 3 μM). Basal, uncoupled, and maximal OCRs were calculated by averaging of the values from each phase [9]. To compare the OCRs in *Lox* and *HKO* hepatocytes, the above assay was performed without TNP.

2.8. Cell culture

Human hepatocyte carcinoma cell line HepG2 (ATCC) and human hepatic stellate cell line LX-2 (provided by Dr. Scott Friedman, Mount Sinai, New York) were cultured in DMEM+1%Pen/Strep+10%FBS.

2.9. HSC activation assay

For quantitative RT-PCR (qRT-PCR) analysis, after 24 h of seeding, the cells (2×10^5 cells/well in a 12-well plate) were serum starved for 24 h and were treated subsequently with TGFβ1−/+ TNP (10 μM) for 24 h.

2.10. RNA isolation and qRT-PCR

RNA isolation and qRT-PCR were conducted as described earlier [27]. Acidic ribosomal protein large P0 *(ARP) mRNA* was used as control and the comparative threshold cycle method was used to calculate changes in mRNA abundance.

2.11. Proteomic studies

The IP6K1-interactome was identified using our published methods [29]. Briefly, IP6K1 was immunoprecipitated from healthy and NASH human liver lysates. Proteins co-precipitated with IgG-IP6K1 and IgG-control were identified by LC-MS/MS. Proteins that were only co-precipitated with IgG-IP6K1 were considered as IP6K1 interactors.

2.12. Protein O-GlcNAcylation studies

Glucose-induced protein O-GlcNAcylation was determined by injecting glucose (2 g/kg body weight, i.p.) or PBS to 16-h-fasted animals [30]. After 4 h, the mice were euthanized and their livers were flash frozen and stored at −80 °C for immunoblot analysis.

2.13. Immunoblotting studies

Tissue and cells were lysed in a RIPA buffer containing a protease-phosphatase inhibitor tablet. Total protein was quantified using a BCA protein assay kit. Equal amounts of total protein were loaded on 10% SDS-PAGE. For collagen detection, a 7% SDS-PAGE was used [31]. Proteins were detected by immunoblotting following our standard protocol [8–10,32]. Densitometric analyses of protein bands were performed using ImageJ software.

2.14. Statistics

Trial/prior experiments were used to determine the sample size with ample statistical power. Animals were excluded if they showed any signs of random sickness. Numbers of mice (*n*) used in experiments are indicated in the legends. Immunoblots were quantified using ImageJ software (NIH). Data are presented as mean ± SEM within dot plots. Each symbol represents an individual sample. For multiple comparisons, one-way or two-way ANOVA with the Holm-Šidák multiple comparison test was used, and for two independent data sets, two-tailed unpaired Student's *t*-test was used. The area under the curve and statistical significance were calculated using GraphPad Prism, 8.2.1.

3. RESULTS

3.1. Hepatocyte-specific *Ip6k1* deletion *(HKO)* protected mice from diet-induced hyperglycemia, hepatic steatosis, and fibrosis

Young (2-month-old), chow-fed *HKO* mice displayed substantially reduced IP6K1 protein in the liver, leaving the other metabolic tissues unaffected (Figure 1A). The residual level of IP6K1 in the *HKO* mouse liver was due to IP6K1's expression in non-parenchymal hepatic cells. *Ip6k2* or *Ip6k3* was not upregulated in *HKO* mouse livers, ruling out the possibility of compensation of *Ip6k1* loss by these isotypes (Fig. S1A). Metabolic profiles of chow-fed *Lox* and *HKO* mice were similar (data not shown). However, *HKO* mice were protected from diet-induced metabolic dysfunction and fibrosis. Insulin- or glucose-mediated glucose disposal (insulin or glucose tolerance test, ITT or GTT) was improved in WD-fed *HKO* mice (Figure 1B–C and Figs. S1B–S1C). Pyruvate and glucagon increase blood glucose levels partly by enhancing hepatic gluconeogenesis, evidenced by an increase in the blood glucose following their injection (pyruvate or glucagon tolerance test, PTT or GgTT). WD-fed *HKO* mice displayed significant decrease in pyruvate- or glucagon-induced rise in blood glucose levels (Figure 1D–E and Figs. S1D–S1E). Moreover, WD-fed *HKO* mouse livers exhibited reduced hepatomegaly, steatosis, and triglyceride (TAG) accumulation (Figure 1F–H) and serum levels of TAG and

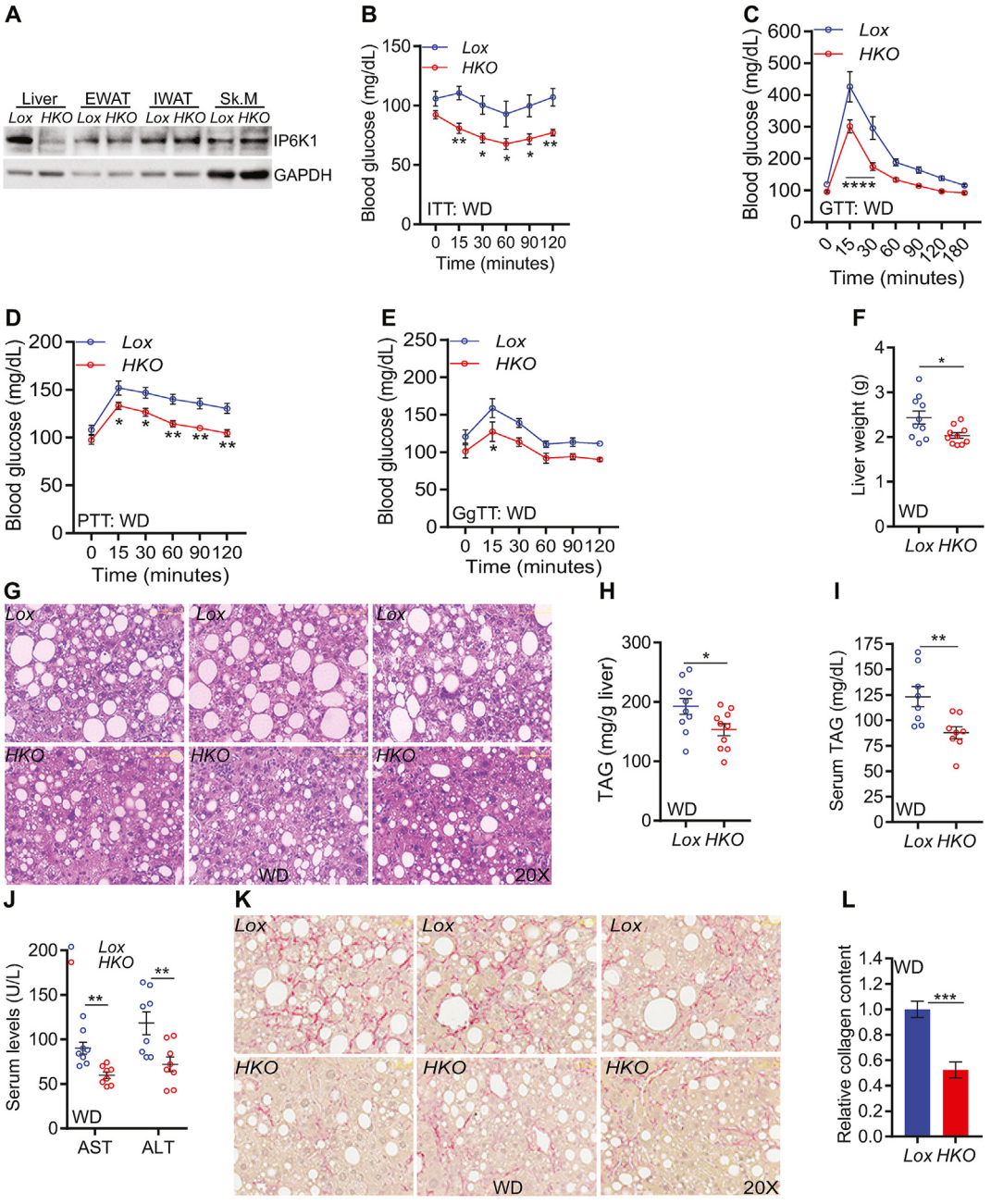

Figure 1: Hepatocyte-specific *Ip6k1* deletion (*HKO*) protected mice from Western diet-induced hyperglycemia, hepatic steatosis, and fibrosis. **A**. *Ip6k1* was deleted in the liver but not in the EWAT, IWAT, or skeletal muscle of *HKO* mice. Data obtained from young, chow-fed mice. **B**. *HKO* mice displayed improved glucose disposal in an insulin tolerance test (ITT). **C**. Glucose-induced peak blood glucose levels were reduced, and its disposal was increased in *HKO* mice (glucose tolerance test, GTT). **D**. *HKO* mice displayed reduced peak blood glucose levels and increased disposal of glucose in a pyruvate tolerance test (PTT). **E**. Glucagon injection increased blood glucose levels to a lesser extent in *HKO* mice (glucagon tolerance test, GgTT). **F**. Liver weight was reduced in *HKO* mice. **G**–**H**. Steatosis and TAG were reduced in *HKO* mouse livers. Representative H&E staining images of 8 mice (n = 8). **I**–**J**. Serum TAG, AST, and ALT levels were reduced in *HKO* mouse livers. **K**–**L**. *HKO* mice displayed reduced fibrosis compared with *Lox* mice. Images are examples from different mice. For comparison of densitometry, the mean value of *Lox* was set as 1 (n = 10 per cohort). Number of mice (*n*) used in each experiment are presented as individual datapoints. WD-fed male mice were used unless otherwise indicated. Data are presented as mean ± SEM within dot plots. For multiple comparisons, two-way ANOVA with the Holm-Šídák multiple comparison test was used, and for two independent data sets, two-tailed unpaired Student's *t*-test was used. $*P < 0.05$, $**P < 0.01$, $***P < 0.001$, $****P < 0.0001$.

hepatotoxicity markers such as aspartate and alanine aminotransferases (AST and ALT) (Figure 1I–J). Chronic hepatocellular metabolic dysfunction provides a stimulus for HSC activation into a fibrogenic phenotype [12–14]. Sirius Red staining of collagen fibers showed that WD-induced hepatic fibrosis was reduced (~40–50%) in *HKO* mouse livers (Figure 1K–L). Expression of *Acta2* (gene for the alpha smooth muscle actin, α-SMA, a marker of HSC activation) was significantly reduced and collagen type 1 alpha 1 and alpha 2 *(Col1a1 and Col1a2)* were moderately diminished, whereas the expression levels of *Col3a1*, the metallopeptidase inhibitor 1 *(Timp1)*, and matrix metalloproteinase 2 *(Mmp2)* were unaltered in WD-fed *HKO* mouse livers (Fig. S1F). Expression of the inflammatory receptor TLR4 and activating

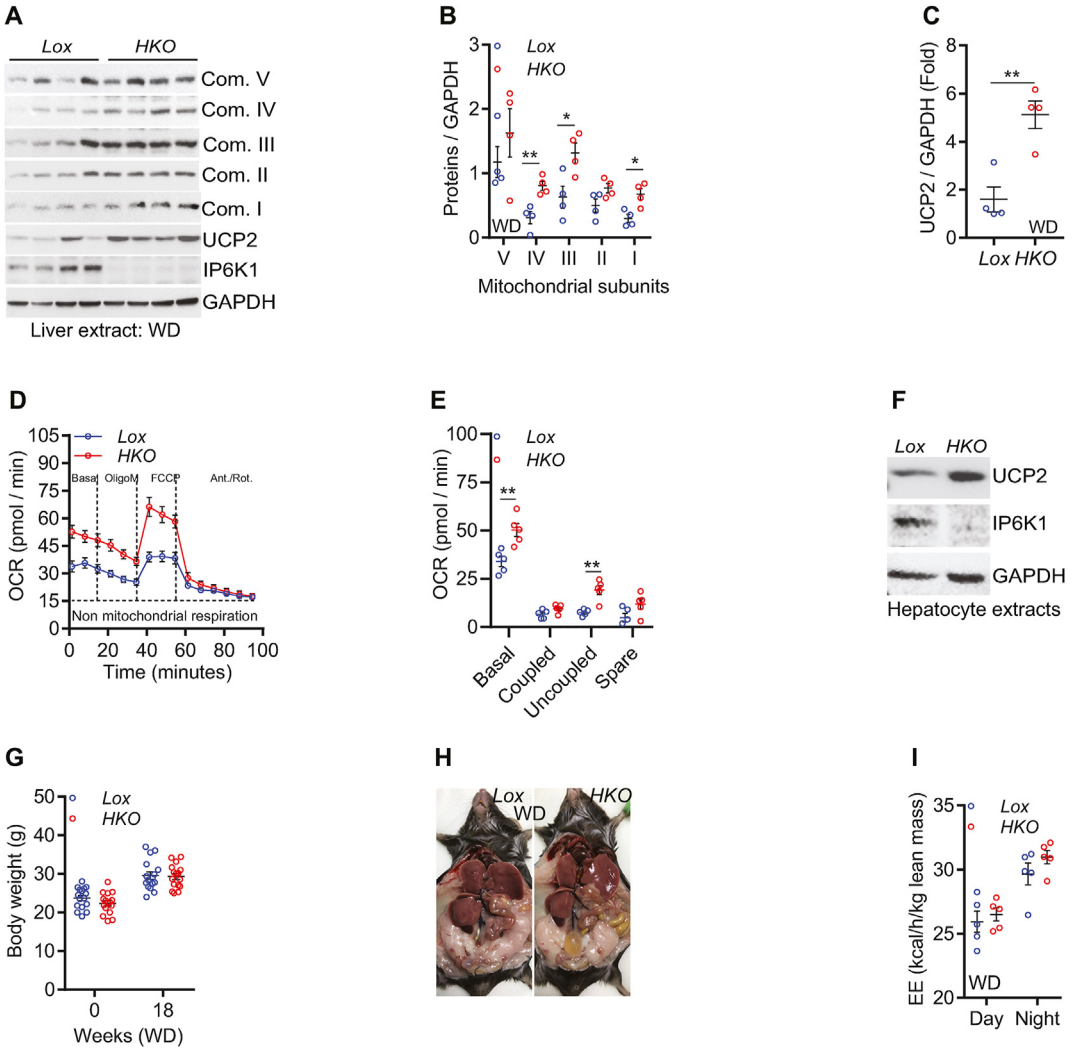

Figure 2: Hepatocyte-specific *Ip6k1 (HKO)* deletion increased mitochondrial oxidative capacity of hepatocytes but did not alter body weight or energy expenditure in mice. **A**—**C.** Hepatic levels of the mitochondrial oxidative phosphorylation proteins (NDUFB8, SDHB, UQCRC2, MTCO1, and ATP5A for complexes I—V, respectively, and UCP2) were augmented in *HKO* mice. **D**—**E.** Hepatocytes isolated from chow-fed *HKO* mice displayed increased OCR *in vitro* due to mitochondrial uncoupling ($n = 5$ experimental replicates). **F.** UCP2 protein level was increased in *HKO* hepatocytes used in Figure 2D. **G**—**H.** Body weight of *Lox* and *HKO* mice were similar at the beginning and end of WD diet feeding and intraabdominal adipose tissue stores in WD-fed mice appeared similar. **I.** Whole body energy expenditure (EE) was similar in *Lox* and *HKO* mice. Number of mice (*n*) used in each experiment are presented as individual datapoints. WD-fed male mice were used unless otherwise indicated. Data are presented as mean ± SEM within dot plots. Hepatocytes were isolated from young, chow-fed male mice. Two-tailed unpaired Student's *t*-test. $*P < 0.05$, $**P < 0.01$.

phosphorylation of the downstream kinase JNK were similar in *Lox* and *HKO* mice (Fig. S1G). Moreover, HFrD feeding developed insulin resistance and mild hepatic steatosis in *Lox* but to a lesser extent in *HKO* mice (Fig. S1H-S1N). This diet did not cause fibrosis in *Lox* or *HKO* mice. Thus, hepatocyte-IP6K1 modulates liver metabolism and the development of NAFLD/NASH.

3.2. Hepatocyte-specific *Ip6k1* deletion *(HKO)* increased mitochondrial oxidative capacity of hepatocytes but did not alter body weight or energy expenditure in mice

Increased uncoupled mitochondrial oxidative capacity in adipocytes reduces fat accumulation in *Ip6k1-KO* mice [9,10]. Similarly, WD-fed *HKO* mouse livers displayed increased levels of hepatic proteins that mediate mitochondrial oxidative capacity including the hepatic isotype of the mitochondrial uncoupling protein UCP2 (Figure 2A—C). Moreover, mitochondrial OCR was increased in *HKO* hepatocytes *in vitro* due to augmented mitochondrial uncoupling (ATP-coupled OCR was unaltered) (Figure 2D—F). Glycolysis (extracellular acidification rate) was also increased in *HKO* hepatocytes (data not shown). Inhibition of the IP6K pathway by the inhibitor TNP [32,33] displayed similar effects in HepG2 and *WT (Lox)* primary hepatocytes (Fig. S2A—S2D). However, localized improvement in hepatocyte energy expenditure was not adequate to alter body weight or whole-body energy expenditure as WD-fed *HKO* mice did not exhibit alterations in these parameters (Figure 2G—I and Figs. S2E—S2G). We observed similar effects in HFD-fed *HKO* mice (data not shown).

3.3. Whole-body deletion of *Ip6k1 (KO)* reduced body weight and robustly protected mice from western diet-induced hyperglycemia, hepatic steatosis, liver injury, and fibrosis

Based on our previous findings with regard to adipocyte deletion of *Ip6k1* [9] and current discoveries with regard to hepatocyte deletion

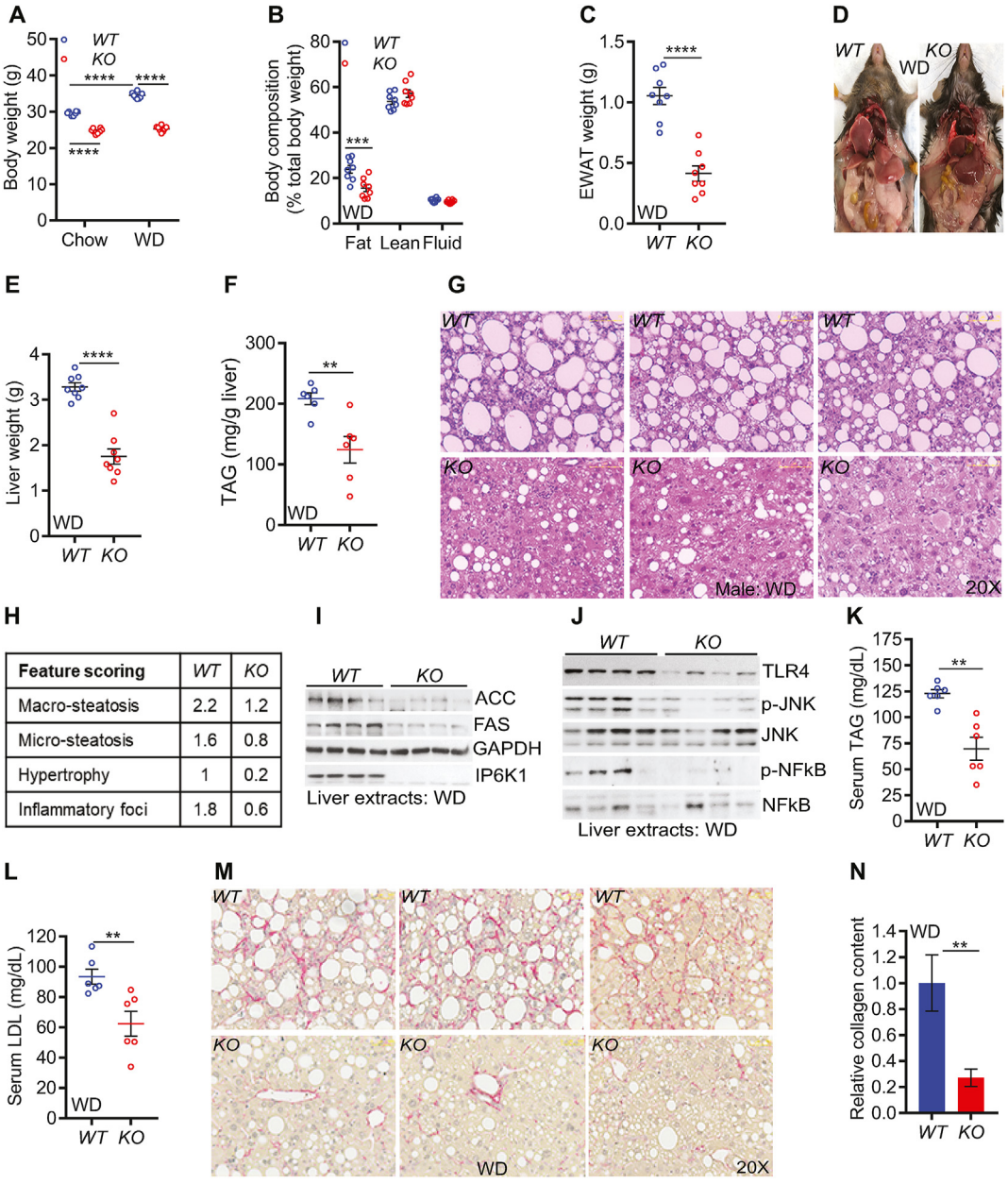

Figure 3: Whole-body deletion of *Ip6k1 (KO)* reduced body weight and robustly protected mice from Western diet-induced hyperglycemia, hepatic steatosis, liver injury, and fibrosis. **A**—**D.** *Ip6k1-KO* males displayed reduced body and fat weight and had darker, normal-appearing livers compared with the pale enlarged livers of *WT* mice. NMR analysis showed a reduction in percent body fat but unaltered lean and fluid masses in the knockouts. **E**—**G.** *Ip6k1-KO* male mice displayed reduced weight and fat accumulation in the liver. **H.** Macro- and micro-steatosis, hepatocyte hypertrophy, and inflammatory foci were reduced in *Ip6k1-KO* mice. NAFLD features were quantified from the H&E slides ($n = 4$ mice per cohort). **I.** The lipogenic ACC and FAS proteins were reduced in *Ip6k1-KO* livers. **J.** TLR4 (normalized to GAPDH in Fig. 3I) and stimulatory phosphorylation of JNK and NFκB were reduced in *Ip6k1-KO* mouse livers. **K**—**L.** Serum TAG and LDL were reduced in *Ip6k1-KO* mice. **M**—**N.** *Ip6k1-KO* mouse livers were robustly protected from fibrosis. For comparison, the mean value of *WT* was set as 1 ($n = 6$ per cohort). Number of mice (n) used in each experiment are presented as individual datapoints. WD-fed male mice were evaluated. Data are presented as mean ± SEM within dot plots. For multiple comparisons, two-way ANOVA with the Holm-Šidák multiple comparison test was used, and for two independent data sets, two-tailed unpaired Student's *t*-test was used. $^{**}P < 0.01$, $^{***}P < 0.001$, $^{****}P < 0.0001$.

of *Ip6k1*, we hypothesized that the improved metabolic phenotype caused by adipocytes lacking *Ip6k1* should protect whole-body *Ip6k1-KO* mice from NAFLD/NASH to a greater extent than hepatocyte deletion alone. WD moderately increased body weight (~5 g) in *WT* but not in whole-body *Ip6k1-KO* male mice (Figure 3A). Accordingly, WD-fed *Ip6k1-KO* mice accumulated less fat (Figure 3B—C and Fig. S3A). WD-fed *Ip6k1-KO* mice also displayed improved glucose disposal following glucose or insulin injections (Fig. S3B—S3E). The livers of *Ip6k1-KO* mice did not have the pale and enlarged appearance of *WT* mice due to reduced TAG accumulation (Figure 3D—G and S3F). Histologic NAFLD feature scoring revealed that micro- and macro-steatosis and hepatocyte hypertrophy were reduced in *Ip6k1-KO* mice (Figure 3H). Levels of the fatty acid biosynthetic enzymes acetyl-CoA carboxylase (ACC) and fatty acid synthase (FAS) were reduced in the *KO* mouse livers (Figure 3I and Fig. S3G). Cholesteryl esters but not free cholesterol levels were

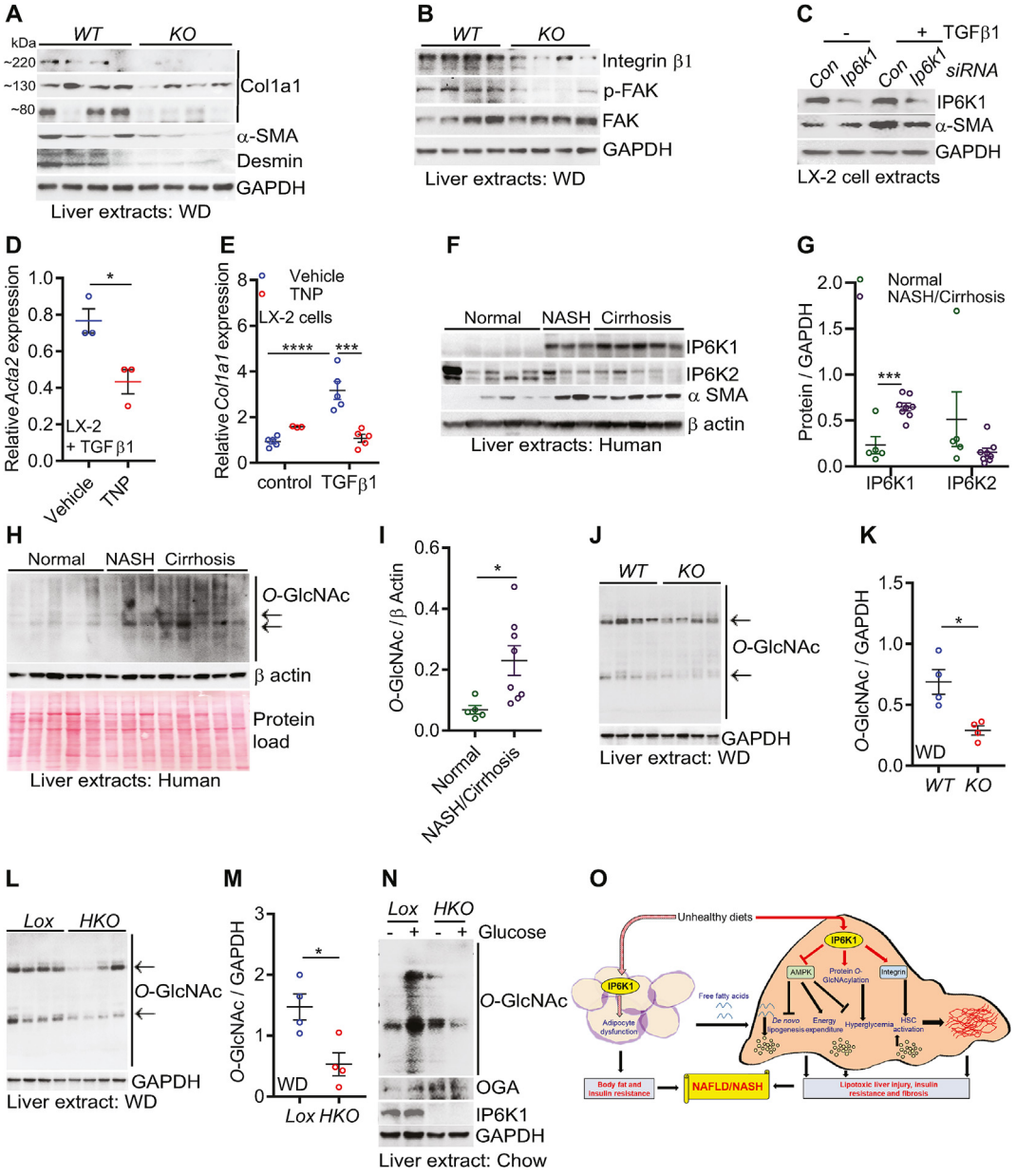

Figure 4: IP6K1 regulates various target proteins and pathways that modulate liver metabolism and fibrosis. **A**. Col1a1, α-SMA, and desmin were reduced in *Ip6k1-KO* mouse livers. For ImageJ analysis of Col1a1, all three Col1a1 bands were compared between *WT* and *Ip6k1-KO* samples. **B.** Integrin β1 and stimulatory phosphorylation of FAK (Y397) were reduced in *Ip6k1-KO* mouse livers. **C.** *Ip6k1* depletion (siRNA) reduced α-SMA protein levels in TGFβ1-treated LX-2 cells. **D.** TNP treatment reduced mRNA expression of *Acta2* in TGFβ1-treated LX-2 cells. **E.** TNP treatment impaired TGFβ1-induced mRNA expression of *Col1a1* in LX-2 cells. **F**—**G.** IP6K1 but not IP6K2 was upregulated in the livers of human NASH and alcoholic cirrhosis patients. α-SMA was used as a marker of profibrogenic stellate cell activation in NASH and cirrhosis. ImageJ quantification was used to compare the expression of proteins in normal vs NASH and cirrhosis livers. **H**—**I.** Levels of protein *O*-GlcNAcylation were increased in human NASH and cirrhosis livers. For quantification, ImageJ analysis was performed on the most prominent *O*-GlcNAcylated bands (indicated by arrows) using β-actin as a control. **J**—**M.** Protein *O*-GlcNAcylation was reduced in WD-fed *Ip6k1-KO* and *HKO* mice compared with control mouse livers. For quantification, ImageJ analysis was performed on two *O*-GlcNAcylated bands that were the most prominent (indicated by arrows). **N.** Glucose-induced protein *O*-GlcNAcylation was reduced in the chow-fed *HKO* mouse liver. **O.** Model showing pleiotropic mechanisms by which IP6K1 promotes the development of NAFLD/NASH. Chronic unhealthy diets stimulate IP6K1-mediated inactivation of AMPK and activation of protein *O*-GlcNAcylation and integrin signaling in the liver. Consequently, mitochondrial oxidative capacity and insulin signaling are impaired, whereas HSCs are activated to a fibrogenic phenotype. IP6K1 also facilitates adipose tissue dysfunction, which causes inappropriate fatty acid release with subsequent uptake in the liver contributing to lipotoxic injury. The net effect is a phenotype of NASH and liver fibrosis. Solid and dotted red arrows denote current and previous discoveries from our group. Back arrows represent information obtained from the literature. Each experiment is presented as individual datapoints. Data are presented as mean ± SEM in dot plots. For multiple comparisons, two-way ANOVA with the Holm-Šidák multiple comparison test was used, and for two independent data sets, two-tailed unpaired Student's *t*-test was used. $^{*}P < 0.05$, $^{***}P < 0.001$, $^{****}P < 0.0001$.

significantly reduced in the *KO* mouse livers (Fig. S3H—S3I). Moreover, *Ip6k1-KO* livers had fewer inflammatory foci, reduced expression of the inflammatory receptor TLR4, and reduced activating phosphorylation of the downstream protein kinases JNK and NFκB (Figure. 3H-last panel, 3J and Fig. S3J—S3K). Serum levels of TAG, low-density lipoprotein (LDL), but not high-density lipoprotein (HDL), cholesterol, AST, and ALT were also lower in WD-fed *Ip6k1-KO* male mice (Figures. 3K—L and S3L—S3M). Consequently, WD-induced hepatic fibrosis was substantially (∼70—80%) reduced in *KO* mouse livers (Figure 3M—N). NAFLD/NASH parameters (insulin resistance, inflammation, hepatic steatosis, and fibrosis) were improved to a greater extent in *Ip6k1-KO* mice than in *HKO* mice compared with those observed in the corresponding control mice. WD-fed *Ip6k1-KO* female mice also gained less body and fat weight (Fig. S3N—S3Q). The livers of female *WT* but not *Ip6k1-KO* mice appeared pale (Fig. S3Q). Liver weight and fat accumulation were marginally less in WD-fed *Ip6k1-KO* females (Figs. S3R-S3S). Yet, *KO* females exhibited significantly reduced serum TAG and ALT levels (Figs. S3T-S3U). WD feeding (for 18 weeks) did not induce fibrosis in *WT* or *Ip6k1-KO* female mice. Thus, due to pleiotropic effects of IP6K1 on various metabolic tissues [6], whole-body *Ip6k1* deletion robustly protected mice from WD-induced weight gain, insulin resistance, metabolic dysfunction, hepatic steatosis, and fibrosis.

3.4. IP6K1 regulates various target proteins and pathways that modulate liver metabolism and fibrosis

IP6K1 regulates various targets and pathways *in vivo* [3,6]. To identify the pathways that were altered in WD-fed *Ip6k1-KO* liver, RNA-Seq studies were performed. Coupled and uncoupled mitochondrial oxidative pathways were upregulated, whereas the gluconeogenic pathway was downregulated, which conform with our observation of improved metabolic phenotypes in *HKO* mice (Table S1, blue and orange denote upregulation and downregulation, respectively; Figs. S4A—B). IP6K1 reduces adipocyte mitochondrial oxidative capacity *via* direct inhibition of AMPK [9,10]. Activating phosphorylation of AMPK was increased in WD-fed *Ip6k1-KO* and *HKO* mouse livers (Figs. S4C—S4D).

RNA-Seq studies also showed that the hepatic transcriptomic profiles of a fibrotic response such as collagen synthesis, HSC activation, integrin signaling and extracellular matrix (ECM) production [13,34] were downregulated in WD-fed *Ip6k1-KO* mouse livers (Table S1 and Fig. S4E). Accordingly, markers of fibrosis and HSC activation such as Col1a1, α-SMA, and desmin were reduced at the protein level in *KO* mouse livers (Figure. 4A and S4F). The integrin receptors activate multiple proteins including the focal adhesion kinase (FAK) to induce the expression of ECM proteins and TGFβ1-induced HSC activation in fibrosis [35,36]. The integrin β1 protein was downregulated and the activating phosphorylation of FAK was decreased in WD-fed *Ip6k1-KO* mouse livers (Figure 4B and S4G—S4H). Based on these results, we checked whether IP6K1 regulates HSC activation. *Ip6k1* and *Ip6k2* were comparably expressed in the human HSC cell line LX-2 under basal and TGFβ1-treated conditions (Fig. S4I), whereas *Ip6k3* was undetectable (data not shown). Interestingly, siRNA-mediated *Ip6k1* depletion reduced the expression of α-SMA in TGFβ1-treated LX-2 cells (Figure 4C). *Ip6k2* depletion did not produce any such effect (data not shown). Moreover, TNP treatment reduced the expression of *Acta2*, the gene for α-SMA (Figure 4D). TNP did not alter *Col1a1* expression under basal conditions but significantly impaired TGFβ1-induced expression of this gene (Figure 4E).

Finally, we assessed the relevance of IP6K1 in human NASH. IP6K1, but not IP6K2, was markedly upregulated in the livers of human NASH and cirrhosis patients, indicating that IP6K1 may play a role in the development and progression of liver fibrosis in humans as it does in mice (Figure 4F—G). LC-MS/MS studies of immunoprecipitated IP6K1 from human livers identified the enzyme *O*-GlcNAcase (OGA) as an IP6K1 interacting protein in NASH (Fig. S4J). OGT (*O*-GlcNAc transferase) and OGA regulate protein *O*-GlcNAcylation by adding and removing the β-D-N-acetylglucosamine (*O*-GlcNAc) moiety to and from target proteins [37,38]. Protein *O*-GlcNAcylation reduces insulin sensitivity, whereas it stimulates lipogenesis [39]. Increased protein *O*-GlcNAcylation was found in the livers of human NASH and cirrhosis patients (Figure 4H—I). Moreover, this modification was reduced in WD-fed *Ip6k1-KO* and *HKO* mouse livers and HFrD-fed *HKO* mouse livers compared with control mice (Figures 4J—M and S4K—S4L). Glucose-induced acute protein *O*-GlcNAcylation [30] was also prevented in chow-fed *HKO* mouse livers (Figure 4N). These results suggest that IP6K1 promotes net protein *O*-GlcNAcylation in the liver.

4. DISCUSSION

Our study demonstrates that hepatocyte-specific *Ip6k1* deletion improves hepatic metabolism, which ameliorates diet-induced hepatic insulin resistance and steatosis in mice. In the liver, IP6K1 regulates various pathways that modulate energy metabolism, insulin sensitivity, and fibrogenesis. Moreover, adipocyte-specific *Ip6k1* deletion enhances thermogenic energy expenditure and reduces β-adrenergic receptor-induced lipolysis, protecting mice from HFD-induced obesity, insulin resistance, and liver fat accumulation [9,10,29]. Furthermore, IP6K1 promotes insulin secretion from pancreatic β cells [7,40], which augments hyperinsulinemia [8], a major contributor to hepatic *de novo* lipogenesis. Thus, the adverse metabolic effects of adipose tissue-derived FFA and hyperinsulinemia are presumably similar in the livers of *Lox* and *HKO* mice. Consequently, *HKO* mice displayed less protection against NAFLD/NASH compared with whole-body *Ip6k1-KO* mice. Based on our previous [8—10] and current studies, we propose a model by which pleiotropic actions of IP6K1 promote the development of NAFLD/NASH (Figure 4O). The albumin-cre deleted *Ip6k1* in hepatocytes and bipotent liver epithelial progenitor cells. To determine the impact of *Ip6k1* deletion specifically on mature hepatocytes, an adeno-associated virus (AAV8-TBG-cre) system should be used in future studies.

IP6K1-regulated other processes may also contribute to NAFLD/NASH development. For example, IP6K1-generated 5-IP7 maintains the cellular polyphosphate levels and pyrophosphorylate protein targets [41,42] that mediate chemotaxis and phagosomal motility of immune cells including macrophages [43,44]. Hence, IP6K1 may also play a role in Kupffer cell-mediated inflammation in NAFLD/NASH. The limited information available suggests the potential significance of other IP6K isotypes in liver and metabolic diseases. Like *Ip6k1*, *Ip6k2* is upregulated in human hepatocellular carcinoma [45]. *Ip6k3* expression is limited to skeletal muscle and heart, and its whole body deletion improves skeletal muscle metabolism, protecting mice from age-induced fat gain and insulin resistance [46].

IP6K1-modulated pathways in metabolic tissues may have therapeutic relevance in NAFLD/NASH. The indirectly acting AMPK-activating drug metformin is first-line therapy for type-2 diabetes (T2DM), and newer direct AMPK-activating drugs are in the clinical development process for the treatment of obesity, T2DM, and NASH [47,48]. Pharmacological activation of whole-body-, and liver-targeted mitochondrial uncoupling is also being evaluated as a therapeutic approach to treat obesity, T2DM, and NAFLD/NASH [49]. Targeting integrin/FAK signaling is a potential strategy to treat fibrotic diseases including

NASH [50]. Increased protein *O*-GlcNAcylation blocks insulin signaling and promotes lipogenesis [39,51]. IP6K1 inhibition may ameliorate metabolic dysfunction and NAFLD/NASH by altering these pathways. Although the mechanisms by which IP6K1 regulates insulin signaling, AMPK, mitochondrial uncoupling, and FAK have been studied [6,8–10,52], how it stimulates protein *O*-GlcNAcylation is currently unknown.

Protein *O*-GlcNAcylation has been shown to differentially influence hepatic metabolism and fibrosis [39,51]. Heterozygous *OGA*-deleted mice (homozygous *OGA*-KO mice do not survive) develop metabolic dysfunction. Moreover, adipocyte-*OGT* deletion reduces protein *O*-GlcNAcylation and ameliorates HFD-induced obesity, insulin resistance, and liver fat accumulation in mice [53,54]. OGT is upregulated in the livers of human NAFLD-associated hepatocellular carcinoma (HCC) and its pharmacological inhibition reduces HCC in a mouse xenograft model [55]. Polyphenolic compounds silibinin and curcumin reduce NAFLD/NASH and protein *O*-GlcNAcylation in mouse models [56,57]. In contrast, decreased protein *O*-GlcNAcylation in human cirrhotic livers and the protective effects of hepatocyte-OGT on alcohol-induced cirrhosis in mice have also been demonstrated [58]. Overall, both activation and disruption of protein *O*-GlcNAcylation have been shown to stimulate HSC activation [59–61]. Perhaps, the regulated modulation of *O*-GlcNAcylation of specific proteins at a particular stage of obesity, insulin resistance, and NASH may have therapeutic importance rather than its constitutive alteration.

Enhancing mitochondrial uncoupling may induce ATP depletion-mediated cellular injury [62]. Moreover, obesity-related fatty liver is not improved by *UCP2* deletion in genetically obese (ob/ob) mice [63]. Encouragingly, pharmacological activation of liver uncoupling by treating mice with DNPME (2,4-dinitrophenol-methyl ether) ameliorates NAFLD without reducing hepatocyte ATP levels [64]. *HKO* hepatocytes showed unaltered coupled (ATP-dependent) OCR (Figure 2E). In *Ip6k1-KO* embryonic fibroblasts, ATP levels are higher due to increased glycolysis [65]. Thus, regulated increases in hepatocyte uncoupling without ATP depletion may have beneficial effects in NAFLD.

In most cases, IP6K1-mediated regulation of its metabolic targets can be attributed to the catalytic activity of IP6K1 [3,6]. Thus, pharmacological inhibition of IP6K1 by the pan-IP6K inhibitor TNP [33] reduces intracellular 5-IP7 [3] levels and ameliorates HFD-induced obesity, hyperinsulinemia, insulin resistance, and liver injury in mice by increasing thermogenic energy expenditure and insulin sensitivity [9,32]. TNP enhances mitochondrial oxidative capacity and insulin sensitivity and reduces fatty acid biosynthesis in adipocytes. It also reduces insulin secretion from β cells and FAK activation in mouse embryonic fibroblasts [9,10,32,33,52,66]. Our current study showed that TNP enhances mitochondrial oxidative capacity of hepatocytes and reduces HSC activation. Unfortunately, TNP is not a drug-like compound due to structural and other shortcomings and thus can only be used as a pharmacological tool [3,32]. Therefore, efforts are ongoing to develop drug-like IP6K inhibitor compounds [67–69]. A newly developed IP6K inhibitor has been shown to alleviate kidney fibrosis in a rat model of chronic kidney disease by increasing ATP and reducing hyperphosphatemia [70]. Hopefully, the improved IP6K inhibitor compounds will be evaluated to assess their potential as treatment targets to reverse NASH and its associated fibrosis.

5. CONCLUSIONS

Pleiotropic actions of IP6K1 in metabolic tissues mediate hepatic metabolic dysfunction leading to NAFLD/NASH. Targeting only the liver is insufficient as a treatment for NAFLD/NASH because it cannot overcome the influences of dysfunctional adipose tissue and perhaps other tissue types throughout the body (e.g., pancreas). Systemic inhibition of IP6K1 or IP6Ks in general could ameliorate the full spectrum of obesity, T2DM, and NAFLD/NASH.

AUTHOR CONTRIBUTIONS

A.C. conceived the project and designed the experiments; A.C. and M.C. generated *HKO* mice; M.C. and S.M. maintained mouse colonies; S.M. performed the majority of the experiments; M.C., B.U, K.M, D.P., E.M., J.H. C.G., and S.G. also performed the experiments; A.C. and S.M. analyzed the majority of the data; B.U., B.N-T., and D.C. analyzed the histology data; J.Z. analyzed RNA-Seq data; D.F. analyzed the lipidomic data; A.C. and S.M. prepared the final figures; A.C. wrote the first draft; B.N-T. edited the draft; B.U and S.M. also helped in the editing. All authors provided input and approved the manuscript prior to submission.

ACKNOWLEDGEMENT

This research was funded by the NIH grant NIDDK-R01DK103746 and the Saint Louis University startup funds to Anutosh Chakraborty, NIH shared and high-end instrumentation grant S10OD025246 to David Ford and Saint Louis University Liver Center support for Barbara Ulmasov. The Proteomics experiments were performed at the Washington University Proteomics Shared Resource (WU-PSR) (R. Reid Townsend MD. Ph.D., director). The expert technical assistance of Petra Erdmann-Gilmore, Yiling Mi, and Rose Connors is gratefully acknowledged. WU-PSR is supported in part by the WU Institute of Clinical and Translational Sciences (NCATS UL1 TR000448), the Mass Spectrometry Research Resource (NIGMS P41 GM103422), and the Siteman Comprehensive Cancer Center Support Grant (NCI P30 CA091842). We thank Dr. Scott Friedman for sharing the LX-2 cells. We also thank Dr. Colin Flaveny, Dr. Subhashis Banerjee, Caroline Murphy and Dr. Grant Kolar at the metabolic and histology core facilities and the members of the Department of Pharmacology and Physiology at the Saint Louis University.

CONFLICT OF INTEREST

B.N-T. has been an advisor or consultant for Alimentiv, Allergan, Allysta, Alnylam, Amgen, Arrowhead, Axcella, Boehringer Ingelheim, BMS, Coherus, Cymabay, Enanta, Fortress, Genfit, Gilead, High Tide, HistoIndex, Innovo, Intercept, Ionis, LG Chem, Lipocine, Madrigal, Medimmune, Merck, Mirum, NGM, NovoNordisk, Novus Therapeutics, pH-Pharma, Sagimet, Target RWE, 89Bio; he has stock options in HepGene and received institutional research grants from Allergan, BMS.

APPENDIX A. SUPPLEMENTARY DATA

Supplementary data to this article can be found online at https://doi.org/10.1016/j.molmet.2021.101364.

REFERENCES

[1] Shears, S.B., 2009. Diphosphoinositol polyphosphates: metabolic messengers? Molecular Pharmacology 76(2):236–252.

[2] Saiardi, A., 2012. Cell signalling by inositol pyrophosphates. Subcellular Biochemistry 59:413–443.

[3] Chakraborty, A., 2018. The inositol pyrophosphate pathway in health and diseases. Biological Reviews of the Cambridge Philosophical Society 93(2): 1203–1227.

[4] Shah, A., Ganguli, S., Sen, J., Bhandari, R., 2017. Inositol pyrophosphates: energetic, omnipresent and versatile signalling molecules. Journal of the Indian Institute of Science 97(1):23–40.

[5] Thomas, M.P., Potter, B.V., 2014. The enzymes of human diphosphoinositol polyphosphate metabolism. FEBS Journal 281(1):14–33.

[6] Mukherjee, S., Haubner, J., Chakraborty, A., 2020. Targeting the inositol pyrophosphate biosynthetic enzymes in metabolic diseases. Molecules 25(6).

[7] Illies, C., Gromada, J., Fiume, R., Leibiger, B., Juhl, K., Yang, S.N., et al., 2007. Requirement of inositol pyrophosphates for full exocytotic capacity in pancreatic beta cells. Science 318(5854):1299–1302.

[8] Chakraborty, A., Koldobskiy, M.A., Bello, N.T., Maxwell, M., Potter, J.J., Juluri, K.R., et al., 2010. Inositol pyrophosphates inhibit Akt signaling, thereby regulating insulin sensitivity and weight gain. Cell 143(6):897–910.

[9] Zhu, Q., Ghoshal, S., Rodrigues, A., Gao, S., Asterian, A., Barrow, J.C., et al., 2016. Adipocyte-specific deletion of Ip6k1 reduces diet-induced obesity by enhancing AMPK-mediated thermogenesis. Journal of Clinical Investigation 126(11):4273–4288.

[10] Zhu, Q., Ghoshal, S., Tyagi, R., Chakraborty, A., 2017. Global IP6K1 deletion enhances temperature modulated energy expenditure which reduces carbohydrate and fat induced weight gain. Molecular Metabolism 6(1):73–85.

[11] Friedman, S.L., Neuschwander-Tetri, B.A., Rinella, M., Sanyal, A.J., 2018. Mechanisms of NAFLD development and therapeutic strategies. Nature Medicine 24(7):908–922.

[12] Brunt, E.M., Wong, V.W.S., Nobili, V., Day, C.P., Sookoian, S., Maher, J.J., et al., 2015. Nonalcoholic fatty liver disease. Nature reviews Disease primers 1:15080.

[13] Tsuchida, T., Friedman, S.L., 2017. Mechanisms of hepatic stellate cell activation. Nature Reviews Gastroenterology & Hepatology 14(7):397–411.

[14] Chakravarthy, M.V., Neuschwander-Tetri, B.A., 2020. The metabolic basis of nonalcoholic steatohepatitis. Endocrinol Diabetes Metab 3(4):e00112.

[15] Brown, M.S., Goldstein, J.L., 2008. Selective versus total insulin resistance: a pathogenic paradox. Cell Metabolism 7(2):95–96.

[16] Jensen, T., Abdelmalek, M.F., Sullivan, S., Nadeau, K.J., Green, M., Roncal, C., et al., 2018. Fructose and sugar: a major mediator of non-alcoholic fatty liver disease. Journal of Hepatology 68(5):1063–1075.

[17] Ioannou, G.N., 2016. The role of cholesterol in the pathogenesis of NASH. Trends in Endocrinology and Metabolism 27(2):84–95.

[18] Loomba, R., Friedman, S.L., Shulman, G.I., 2021. Mechanisms and disease consequences of nonalcoholic fatty liver disease. Cell 184(10):2537–2564.

[19] Neuschwander-Tetri, B.A., 2020. Therapeutic landscape for NAFLD in 2020. Gastroenterology 158(7):1984–1998.e3.

[20] Konerman, M.A., Jones, J.C., Harrison, S.A., 2018. Pharmacotherapy for NASH: current and emerging. Journal of Hepatology 68(2):362–375.

[21] Wolf, M.J., Adili, A., Piotrowitz, K., Abdullah, Z., Boege, Y., Stemmer, K., et al., 2014. Metabolic activation of intrahepatic CD8+ T cells and NKT cells causes nonalcoholic steatohepatitis and liver cancer via cross-talk with hepatocytes. Cancer Cell 26(4):549–564.

[22] Yang, Y.M., Noureddin, M., Liu, C., Ohashi, K., Kim, S.Y., Ramnath, D., et al., 2019. Hyaluronan synthase 2-mediated hyaluronan production mediates Notch1 activation and liver fibrosis. Science Translational Medicine 11(496).

[23] Malehmir, M., Pfister, D., Gallage, S., Szydlowska, M., Inverso, D., Kotsiliti, E., et al., 2019. Platelet GPIbα is a mediator and potential interventional target for NASH and subsequent liver cancer. Nature Medicine 25(4):641–655.

[24] Kim, M.S., Krawczyk, S.A., Doridot, L., Fowler, A.J., Wang, J.X., Trauger, S.A., et al., 2016. ChREBP regulates fructose-induced glucose production independently of insulin signaling. Journal of Clinical Investigation 126(11):4372–4386.

[25] McCommis, K.S., Chen, Z., Fu, X., McDonald, W.G., Colca, J.R., Kletzien, R.F., et al., 2015. Loss of mitochondrial pyruvate carrier 2 in the liver leads to defects in gluconeogenesis and compensation via pyruvate-alanine cycling. Cell Metabolism 22(4):682–694.

[26] Liang, W., Menke, A.L., Driessen, A., Koek, G.H., Lindeman, J.H., Stoop, R., et al., 2014. Establishment of a general NAFLD scoring system for rodent models and comparison to human liver pathology. PLoS One 9(12):e115922.

[27] Ulmasov, B., Noritake, H., Carmichael, P., Oshima, K., Griggs, D.W., Neuschwander-Tetri, B.A., et al., 2019. An inhibitor of arginine-glycine-aspartate-binding integrins reverses fibrosis in a mouse model of nonalcoholic steatohepatitis. Hepatol Commun 3(2):246–261.

[28] Yu, H., Rimbert, A., Palmer, A.E., Toyohara, T., Xia, Y., Xia, F., et al., 2019. GPR146 deficiency protects against hypercholesterolemia and atherosclerosis. Cell 179(6):1276–1288 e14.

[29] Ghoshal, S., Tyagi, R., Zhu, Q., Chakraborty, A., 2016. Inositol hexakisphosphate kinase-1 interacts with perilipin1 to modulate lipolysis. The International Journal of Biochemistry & Cell Biology 78:149–155.

[30] Guinez, C., Filhoulaud, G., Rayah-Benhamed, F., Marmier, S., Dubuquoy, C., Dentin, R., et al., 2011. O-GlcNAcylation increases ChREBP protein content and transcriptional activity in the liver. Diabetes 60(5):1399–1413.

[31] Martínez-Salgado, C., Fuentes-Calvo, I., García-Cenador, B., Santos, E., López-Novoa, J.M., 2006. Involvement of H- and N-Ras isoforms in transforming growth factor-beta1-induced proliferation and in collagen and fibronectin synthesis. Experimental Cell Research 312(11):2093–2106.

[32] Ghoshal, S., Zhu, Q., Asteian, Lin, H., Xu, H., Ernst, G., et al., 2016. TNP [N2-(m-Trifluorobenzyl), N6-(p-nitrobenzyl)purine] ameliorates diet induced obesity and insulin resistance via inhibition of the IP6K1 pathway. Mol Metab 5(10):903–917.

[33] Padmanabhan, U., Dollins, D.E., Fridy, York, J.D., Downes, C.P., 2009. Characterization of a selective inhibitor of inositol hexakisphosphate kinases: use in defining biological roles and metabolic relationships of inositol pyrophosphates. Journal of Biological Chemistry 284(16):10571–10582.

[34] Schwabe, R.F., Tabas, I., Pajvani, U.B., 2020. Mechanisms of fibrosis development in nonalcoholic steatohepatitis. Gastroenterology 158(7):1913–1928.

[35] Zhao, X.K., Yu, L., Cheng, M.L., Che, P., Lu, Y.Y., Zhang, Q., et al., 2017. Focal adhesion kinase regulates hepatic stellate cell activation and liver fibrosis. Scientific Reports 7(1):4032.

[36] Kim, K.K., Sheppard, D., Chapman, H.A., 2018. TGF-β1 signaling and tissue fibrosis. Cold Spring Harb Perspect Biol 10(4).

[37] Chatham, J.C., Zhang, J., Wende, A.R., 2021. Role of O-linked N-acetylglucosamine protein modification in cellular (Patho)Physiology. Physiological Reviews 101(2):427–493.

[38] Hart, G.W., Slawson, C., Ramirez-Correa, G., Lagerlof, O., 2011. Cross talk between O-GlcNAcylation and phosphorylation: roles in signaling, transcription, and chronic disease. Annual Review of Biochemistry 80:825–858.

[39] Zhang, K., Yin, R., Yang, X., O-GlcNAc, 2014. A bittersweet switch in liver. Frontiers in Endocrinology 5:221.

[40] Bhandari, R., Juluri, K.R., Resnick, A.C., Snyder, 2008. Gene deletion of inositol hexakisphosphate kinase 1 reveals inositol pyrophosphate regulation of insulin secretion, growth, and spermiogenesis. Proceedings of the National Academy of Sciences of the U S A 105(7):2349–2353.

[41] Saiardi, A., 2012. How inositol pyrophosphates control cellular phosphate homeostasis? Adv Biol Regul 52(2):351–359.

[42] Saiardi, A., Bhandari, R., Resnick, A.C., Snowman, A.M., Snyder, S.H., 2004. Phosphorylation of proteins by inositol pyrophosphates. Science 306(5704):2101–2105.

[43] Chanduri, M., Rai, A., Malla, A.B., Wu, M., Fiedler, D., Mallik, R., 2016. Inositol hexakisphosphate kinase 1 (IP6K1) activity is required for cytoplasmic dynein-driven transport. Biochemical Journal 473(19):3031–3047.

[44] Hou, Q., Liu, F., Chakraborty, A., Jia, Y., Prasad, A., Yu, H., et al., 2018. Inhibition of IP6K1 suppresses neutrophil-mediated pulmonary damage in bacterial pneumonia. Science Translational Medicine 10(435).

[45] Nwosu, Z.C., Megger, D.A., Hammad, S., Sitek, B., Roessler, S., Ebert, M.P., et al., 2017. Identification of the consistently altered metabolic targets in human hepatocellular carcinoma. Cell Mol Gastroenterol Hepatol 4(2):303–323.e1.

[46] Moritoh, Y., Oka, M., Yasuhara, Y., Hozumi, H., Iwachidow, K., Fuse, H., et al., 2016. Inositol hexakisphosphate kinase 3 regulates metabolism and lifespan in mice. Scientific Reports 6:32072.

[47] Esquejo, R.M., Salatto, C.T., Delmore, J., Albuquerque, B., Reyes, A., Shi, Y., et al., 2018. Activation of liver AMPK with PF-06409577 corrects NAFLD and lowers cholesterol in rodent and primate preclinical models. EBioMedicine 31:122—132.

[48] Liang, Z., Li, T., Jiang, S., Xu, J., Di, W., Yang, Z., et al., 2017. AMPK: a novel target for treating hepatic fibrosis. Oncotarget 8(37):62780—62792.

[49] Goedeke, L., Perry, R.J., Shulman, G.I., 2019. Emerging pharmacological targets for the treatment of nonalcoholic fatty liver disease, insulin resistance, and type 2 diabetes. Annual Review of Pharmacology and Toxicology 59:65—87.

[50] Lagares, D., Kapoor, M., 2013. Targeting focal adhesion kinase in fibrotic diseases. BioDrugs 27(1):15—23.

[51] Mueller, T., Ouyang, X., Johnson, M.S., Qian, W.J., Chatham, J.C., Darley-Usmar, V., et al., 2021. New insights into the biology of protein O-GlcNAcylation: approaches and observations. Frontiers in Aging 1(5).

[52] Fu, C., Xu, J., Cheng, W., Rojas, T., Chin, A.C., Snowman, A.M., et al., 2017. Neuronal migration is mediated by inositol hexakisphosphate kinase 1 via alpha-actinin and focal adhesion kinase. Proceedings of the National Academy of Sciences of the U S A 114(8):2036—2041.

[53] Keembiyehetty, C., Love, D.C., Gavrilova, O., Comly, M.E., Harwood, K.R., Hanover, J.A., 2015. Conditional knock-out reveals a requirement for O-linked N-Acetylglucosaminase (O-GlcNAcase) in metabolic homeostasis. Journal of Biological Chemistry 290(11):7097—7113.

[54] Li, M.D., Vera, N.B., Yang, Y., Zhang, B., Ni, W., Ziso-Qejvanaj, E., et al., 2018. Adipocyte OGT governs diet-induced hyperphagia and obesity. Nature Communications 9(1):5103.

[55] Xu, W., Zhang, X., Wu, J.L., Fu, L., Liu, K., Liu, D., et al., 2017. O-GlcNAc transferase promotes fatty liver-associated liver cancer through inducing palmitic acid and activating endoplasmic reticulum stress. Journal of Hepatology 67(2):310—320.

[56] Lee, S.J., Nam, M.J., Lee, D.E., Park, J.W., Kang, B.S., Lee, D.S., et al., 2018. Silibinin ameliorates O-GlcNAcylation and inflammation in a mouse model of nonalcoholic steatohepatitis. International Journal of Molecular Sciences 19(8).

[57] Lee, D.E., Lee, S.J., Kim, S.J., Lee, H.S., Kwon, O.S., 2019. Curcumin ameliorates nonalcoholic fatty liver disease through inhibition of O-GlcNAcylation. Nutrients 11(11).

[58] Zhang, B., Li, M.D., Yin, R., Liu, Y., Yang, Y., Mitchell-Richards, K.A., et al., 2019. O-GlcNAc transferase suppresses necroptosis and liver fibrosis. JCI Insight 4(21).

[59] Kohda, Y., Kanematsu, M., Kono, T., Terasaki, F., Tanaka, T., 2009. Protein O-glycosylation induces collagen expression and contributes to diabetic cardiomyopathy in rat cardiac fibroblasts. Journal of Pharmacological Sciences 111(4):446—450.

[60] Fan, X., Chuan, S., Hongshan, W., 2013. Protein O glycosylation regulates activation of hepatic stellate cells. Inflammation 36(6):1248—1252.

[61] Li, R., Ong, Q., Wong, C.C., Chu, E.S., Sung, Yang, X., et al., 2021. O-GlcNAcylation inhibits hepatic stellate cell activation. Journal of Gastroenterology and Hepatology.

[62] Cortez-Pinto, H., Machado, M.V., 2009. Uncoupling proteins and non-alcoholic fatty liver disease. Journal of Hepatology 50(5):857—860.

[63] Baffy, G., Zhang, C.Y., Glickman, J.N., Lowell, B.B., 2002. Obesity-related fatty liver is unchanged in mice deficient for mitochondrial uncoupling protein 2. Hepatology 35(4):753—761.

[64] Perry, R.J., Kim, T., Zhang, X.M., Lee, H.Y., Pesta, D., Popov, V.B., et al., 2013. Reversal of hypertriglyceridemia, fatty liver disease, and insulin resistance by a liver-targeted mitochondrial uncoupler. Cell Metabolism 18(5):740—748.

[65] Szijgyarto, Z., Garedew, A., Azevedo, C., Saiardi, A., 2011. Influence of inositol pyrophosphates on cellular energy dynamics. Science 334(6057):802—805.

[66] Jadav, R.S., Kumar, D., Buwa, N., Ganguli, S., Thampatty, S.R., Balasubramanian, N., et al., 2016. Deletion of inositol hexakisphosphate kinase 1 (IP6K1) reduces cell migration and invasion, conferring protection from aerodigestive tract carcinoma in mice. Cellular Signalling 28(8):1124—1136.

[67] Puhl-Rubio, A.C., Stashk, M.A., Wang, H., Hardy, P.B., Tyagi, V., Li, B., et al., 2018. Use of protein kinase-focused compound libraries for the discovery of New inositol phosphate kinase inhibitors. SLAS Discov, 2472555218775323.

[68] Gu, C., Stashko, M.A., Puhl-Rubio, A.C., Chakraborty, M., Chakraborty, A., Frye, S.V., et al., 2019. Inhibition of inositol polyphosphate kinases by quercetin and related flavonoids: a structure-activity analysis. Journal of Medicinal Chemistry.

[69] Liao, G., Ye, W., Heitmann, T., Ernst, G., DePasquale, M., Xu, L., et al., 2021. Identification of small-molecule inhibitors of human inositol hexakisphosphate kinases by high-throughput screening. ACS Pharmacol Transl Sci 4(2):780—789.

[70] Moritoh, Y., Abe, S.I., Akiyama, H., Kobayashi, A., Koyama, Hara, R., et al., 2021. The enzymatic activity of inositol hexakisphosphate kinase controls circulating phosphate in mammals. Nature Communications 12(1):4847.

